COMMUNICATION

Check for updates

Graphene oxide nanosheets modulate spinal glutamatergic transmission and modify locomotor behaviour in an *in vivo* zebrafish model†

Giada Cellot, [ID] ‡*[a] Sandra Vranic, [ID] [b] Yuyoung Shin, [ID] [c] Robyn Worsley,[c] Artur Filipe Rodrigues, [ID] [b] Cyrill Bussy, [ID] [b] Cinzia Casiraghi, [ID] [c] Kostas Kostarelos [ID] [b] and Jonathan Robert McDearmid[a]

Graphene oxide (GO), an oxidised form of graphene, is widely used for biomedical applications, due to its dispersibility in water and simple surface chemistry tunability. In particular, small (less than 500 nm in lateral dimension) and thin (1–3 carbon monolayers) graphene oxide nanosheets (s-GO) have been shown to selectively inhibit glutamatergic transmission in neuronal cultures *in vitro* and in brain explants obtained from animals injected with the nano-material. This raises the exciting prospect that s-GO can be developed as a platform for novel nervous system therapeutics. It has not yet been investigated whether the interference of the nanomaterial with neurotransmission may have a downstream outcome in modulation of behaviour depending specifically on the activation of those synapses. To address this problem we use early stage zebrafish as an *in vivo* model to study the impact of s-GO on nervous system function. Microinjection of s-GO into the embryonic zebrafish spinal cord selectively reduces the excitatory synaptic transmission of the spinal network, monitored *in vivo* through patch clamp recordings, without affecting spinal cell survival. This effect is accompanied by a perturbation in the swimming activity of larvae, which is the locomotor behaviour generated by the neuronal network of the spinal cord. Such results indicate that the impact of s-GO on glutamate based neuronal transmission is preserved *in vivo* and can induce changes in animal behaviour. These findings pave the way for use of s-GO as a modulator of nervous system function.

New concepts

Nanomaterials, including small graphene oxide nanoflakes (s-GO), are artificial materials with at least one dimension in the nanometer scale. Thanks to this characteristic, they are suited to interact with the smallest components of the brain, such as synapses, suggesting their use as tool for manipulating neuronal function. This might be exploited for the development of innovative nanomaterial-based medical devices, to recover pathologically altered neuronal activity.Respect to previous *in vitro* and *in vivo* studies which have demonstrated the ability of s-GO in downregulating excitatory synapses, here we explore whether s-GO interference with neurotransmission might have as a downstream outcome the modulation of behaviour that relies on the activation of the nanomaterial exposed synapses.We report that, once injected in the spinal cord of zebrafish larvae, s-GO changed the electrical activity of neurons located in this part of the nervous system and modified the locomotor behaviour of fish, which depends on spinal network activity. Thus, we validated zebrafish as *in vivo* model to study nanomaterial–neuron interaction, providing evidence that s-GO might be used as a modulator of synaptic activity and related behaviour. This paves the way toward the development of novel biomedical applications for graphene related nanomaterials.

1. Introduction

Graphene is a two-dimensional nanomaterial characterized by a honeycomb-lattice structure made of sp[2]-hybridized carbon atoms. In addition to its use in a range of industrial sectors, graphene's tunable properties[1,2] have garnered interest as a tool for biomedical applications.[3–7] These include the development of neuronal implants and biodevices in the field of neuroscience research and medicine.[8,9] A particular derivative of graphene, called graphene oxide (GO), which contains carbon, oxygen and hydrogen in variable ratios has attracted a lot of attention for healthcare applications,[3] mainly due to its facile aqueous dispersion and the availability of C–O groups. Recent *in vitro* studies of neuronal cultures have shown that small lateral dimension GO (s-GO, with lateral size of less than 500 nm and thickness of 1–3 carbon monolayers), can modify synaptic activity without affecting neuronal survival.[10] In this study, chronic s-GO treatment induced a specific downregulation of excitatory glutamatergic transmission in cultured rat hippocampal neurons[10] and reduced glutamate content in synaptic

[a] *Department of Neuroscience, Psychology and Behaviour, College of Life Sciences, University of Leicester, Leicester, LE1 7RH, UK*

[b] *Nanomedicine Lab, Faculty of Biology, Medicine & Health and National Graphene Institute, University of Manchester, AV Hill Building, Manchester M13 9PT, UK*

[c] *Department of Chemistry, University of Manchester, Manchester M13 9PL, UK*

† Electronic supplementary information (ESI) available. See DOI: 10.1039/c9nh00777f

‡ Current address: International School for Advanced Studies (SISSA), via Bonomea n. 256 Trieste, Italy. E-mail: cellot@sissa.it

vesicles.[10,11] More recently, the ability of s-GO in promoting a significant reduction in excitatory synaptic transmission was detected also in hippocampal explants obtained from animals injected 48 hours before with the nanomaterial.[12]

The potential of s-GO to downregulate excitatory transmission raises the exciting prospect that these materials can be exploited for treatment of disorders involving a pathological increase in glutamate synaptic transmission. Glutamate is the main excitatory neurotransmitter of the vertebrate brain[13] and excessive glutamate signalling can result in excitotoxicity.[14] Indeed, glutamate excitotoxicity has been implicated in the pathogenesis of many neurological disorders including Huntington's, Parkinson's and Alzheimer's disease, epilepsy, amyotrophic lateral sclerosis, pain and anxiety disorders.[14–19] However, before the therapeutic potential of this material can be determined, its effects on neurotransmission at glutamatergic synapses must be validated *in vivo* by valuing also its possible impact on behaviour that relies on the activation of those synapses. To this end, we have used larval zebrafish as an *in vivo* model for studying the effect of nanomaterials on glutamate based synaptic communication. Furthermore, we investigated the impact of s-GO on the locomotor behaviour that correlates with the neuronal network activity of the spinal cord, the structure where s-GO were delivered. Early stage zebrafish are ideally suited for this purpose as they are amenable to a broad range of *in vivo* methodologies, including patch clamp electrophysiology, confocal imaging and behavioural analysis.[20,21] In addition, the accessibility and relative simplicity of the zebrafish spinal cord[22] coupled with detailed knowledge of spinal neuron anatomy and function[23–28] makes this an attractive system for exploring the effect of carbon-based nanomaterials on synaptic function and behaviour.

Here we show that s-GO nanosheets delivered to the spinal cord of zebrafish larvae were able to selectively reduce spinal glutamatergic transmission *in vivo* without affecting neuronal survival. Patch clamp recordings performed *in vivo* two days after intra-spinal delivery of s-GO resulted in a strong reduction in glutamate release at excitatory synapses of spinal motor neurons. Such phenomenon was detected also during fictive swimming (that is the spinal electrical activity that correlates with bouts of locomotor behaviour in paralysed fish) in terms of a decrease in glutamatergic inputs received by motor neurons. These effects were accompanied by a decrease in the locomotor performance during behavioural experiments. Moreover, the observed changes were specific for s-GO, since the treatment with defects-free graphene (dfG) of similar size did not affect synaptic transmission or locomotor behaviour of injected larvae, suggesting that the effect may be related to the specific surface chemistry and dimensionality of s-GO. Our results provide the first demonstration that s-GO, by interfering with synaptic signalling of the brain region where they are delivered *in vivo*, can be used as a modulator of the behaviour emerging from the activity of the synapses exposed to the nanomaterial.

2. Results

2.1. Characterization of nanomaterials

Two types of graphene-based materials, dfG and s-GO, were used in this study.

s-GO were synthesized using a modified Hummers approach (see ESI†), following previously established protocols to ensure the production of endotoxin-free dispersions.[10,29–31] The resulting s-GO dispersion had a brownish colour and showed good colloidal stability in aqueous media, as well as chemical stability at room temperature for more than 6 months. The physicochemical characterization of s-GO has already been reported elsewhere[30] and is summarized in Table 1 and in Fig. S1a and c (ESI†). Morphology of s-GO nanosheets was examined by transmission electron microscopy (TEM) and atomic force microscopy (AFM), showing that the average lateral dimensions of s-GO are between 150–200 nm. Flakes were determined to be 1–3 layers thick (Table 1 and Fig. S1a and c, ESI†).

dfG were produced by liquid-phase exfoliation of graphite[33] in water, using 1-pyrenesulfonic acid sodium salt as stabilizer.[32] The dfG dispersions in aqueous media were homogeneous, of black colour, and stable at room temperature for at least 6 months. The physicochemical characterization of the dfG dispersions has already been reported elsewhere[32] and is summarized in Table 1 and in Fig. S1b, d (ESI†). Structural properties were studied by TEM and AFM, showing that the average lateral dimensions of dfG are between 50–500 nm (Table 1 and Fig. S1b, d, ESI†), which are comparable to s-GO. Thickness of the flakes was found to be between 1 and 20 layers, using the AFM data and assuming a nominal thickness of ~ 5 nm, considering the layer of absorbed molecules on both sides of the graphene nanosheet.[32]

Table 1 Physicochemical characteristics of graphene based materials used in this study

	Technique	s-GO	dfG
Lateral dimensions[a]	AFM	30–700 nm	30–500 nm
Thickness[a]	AFM	1–3 layers	1–20 layers
Degree of defects (I_D/I_G)[c]	Raman spectroscopy	1.35 ± 0.03	0.75 ± 0.3
Surface charge	ζ-Potential	-55.0 ± 0.8 mV	-36.2 ± 1.1 mV
Chemical composition (purity)	XPS	C: 67.8%, O: 31.8%, N: 0.4%, Na: 0.1% (99.5%)	C: 94.5%, O: 5.2%,[b] S: 0.3%
C : O ratio	XPS	2.1	—
π–π,[a] O=C–O, C=O, C–O, C–C & C=C	XPS	0.3%, 5.0%, 5.1%, 49.2%, 41.4%	—

[a] Lateral dimensions and thickness are reported as a range between the minimum and the maximum size detected. [b] Adventitious contamination during XPS sample preparation. [c] Measured at 633 nm excitation wavelength.

2.2. dfG and s-GO do not affect zebrafish development, neuronal survival or the passive electrical properties of motor neurons

To determine the biocompatibility of graphene-based materials *in vivo*, a saline solution containing 0.5 ng of dfG or s-GO was microinjected into the spinal cord of zebrafish at two days post fertilization (dpf; Fig. 1a). For controls, age-matched fish from the same clutch were microinjected with saline solution. Two days after injection, larval development was studied by measuring anatomical features that are commonly used to assess the degree of maturation[34] (Fig. 1b). Fish injected with dfG and s-GO appeared morphologically identical to controls (Fig. 1c) and exhibited no statistically significant variation in total body length (control: 3.5 ± 0.1 mm, $n = 10$ fish; dfG-injected: 3.4 ± 0.1 mm, $n = 11$ fish; s-GO-injected: 3.6 ± 0.1 mm, $n = 10$ fish), height measured at the level of the urogenital pore (control: 0.22 ± 0.01 mm, dfG-injected: 0.20 ± 0.01 mm and s-GO-injected: 0.23 ± 0.01 mm), yolk sac diameter (control: 0.50 ± 0.02 mm, dfG-injected: 0.48 ± 0.02 mm, and s-GO-injected: 0.49 ± 0.01 mm) or eye size (control: 0.29 ± 0.01 mm, dfG-injected: 0.26 ± 0.01 mm and s-GO-injected: 0.27 ± 0.01 mm; P values > 0.05, Fig. 1d). Thus, injection of these materials did not grossly impact morphological development.

We next assessed the effect of nanomaterials on neuron survival (Fig. 1e). To do this, transgenic fish that selectively express GFP in motor neurons (Tg(hb9:GFP)),[35] glycinergic (Tg(glyT2:GFP)) or glutamatergic interneurons (Tg(VGLUT2A:GFP))[36] were injected with control or nanomaterial-containing solution. Two days after injection, the number of GFP-positive neurons was quantified in two segments of the spinal cord around the site of injection. The mean number of motor neurons did not significantly differ between control, dfG and s-GO injected larvae (control: 119 ± 6 cells, $n = 11$ fish, dfG-injected: 118 ± 6 cells, $n = 12$ fish and s-GO-injected: 113 ± 3 cells, $n = 15$ fish; P value > 0.05, Fig. 1f). Similarly, no differences were observed in the number of inhibitory glycinergic (control: 91 ± 4 cells, $n = 7$ fish, dfG-injected: 81 ± 3 cells, $n = 7$ fish and s-GO-injected: 84 ± 5 cells, $n = 7$ fish) or excitatory glutamatergic (control: 129 ± 10 cells, $n = 9$ fish, dfG-injected: 126 ± 15 cells, $n = 7$ fish and s-GO-injected: 136 ± 11 cells, $n = 7$ fish) interneurons among the different treatments ($P > 0.05$). These observations strongly suggest that nanomaterial injection did not modify survival of neurons in the zebrafish spinal cord.

Next, we performed patch clamp electrophysiology of GFP-labelled motor neurons to determine whether nanomaterial injection affected the membrane properties of these cells (Fig. 1g). We targeted specifically primary motor neurons for this purpose, as these have well-characterized and stereotyped soma size, soma position and axonal morphology.[37,38]

When comparing control ($n = 19$ cells), dfG-injected ($n = 11$ cells) and s-GO-injected ($n = 20$ cells) fish (Fig. 1h), no statistically significant difference in cell capacitance (control: 20 ± 1 pF, dfG-injected: 17 ± 1 pF; s-GO-injected: 19 ± 1 pF, $P > 0.05$), input resistance (control: 126 ± 10 MΩ; dfG-injected: 169 ± 19 MΩ; s-GO-injected: 145 ± 14 MΩ, $P > 0.05$) or resting membrane

potential (control: −70 ± 1 mV; dfG-injected: −69 ± 1 mV; s-GO-injected: −68 ± 1 mV, $P > 0.05$) was observed. Therefore, these basic indicators of neuronal maturation and health[39–41] are not changed by exposure to nanomaterials. In summary, these results suggest that the direct microinjection of the two types of graphene-based nanomaterials did not affect the development, gross morphology of zebrafish and had no effect on the survival and basic physiological properties of motor neurons.

2.3. s-GO selectively reduce glutamatergic synaptic transmission

We next studied the effect of s-GO and dfG on synaptic glutamatergic and glycinergic transmission in the spinal cord. To this end, we injected fish with nanomaterials and, after a two-days incubation period, conducted whole cell patch clamping of primary motor neurons (using the experimental setting shown in Fig. 1g). We began by analysing miniature postsynaptic currents (mPSCs) in the presence of tetrodotoxin (1 μM), a Na⁺ channel blocker that abolishes spike-dependent transmission. Under this condition, neurotransmitter containing vesicles are released stochastically from the presynaptic terminal, making neurotransmitter molecules available in the synaptic cleft to bind their receptors expressed on postsynaptic membrane. The properties of mPSCs can be used to derive information about the synapse structural and functional characteristics: changes in mPSCs frequency are usually related to modifications in the presynaptic release probability and/or in the number of synaptic contacts, while mPSCs amplitude is dependent on postsynaptic factors.[12]

Glutamatergic (glut-) mPSCs were pharmacologically isolated by bath application of picrotoxin (50 μM) and strychnine (1 μM), which block GABAergic and glycinergic currents respectively (Fig. 2a). Analysis revealed a significant reduction in the frequency of glut-mPSCs in s-GO injected fish (1.0 ± 0.2 Hz, $n = 20$ cells, $P = 0.024$) when compared to control fish (2.0 ± 0.4 Hz, $n = 19$ cells). However, the amplitude (control: 12 ± 1 pA and s-GO-injected: 10 ± 1 pA), rise time (control: 0.28 ± 0.01 ms and s-GO-injected: 0.31 ± 0.02 ms) and decay time (control: 0.87 ± 0.04 ms and s-GO-injected: 0.90 ± 0.04 ms) of glu-mPSCs were not affected ($P > 0.05$). The finding was specific for s-GO, as fish injected with dfG exhibited no changes in glut-mPSCs frequency (1.4 ± 0.4 Hz), amplitude (14 ± 2 pA) or kinetics (rise time was 0.31 ± 0.02 ms and decay time was 1.08 ± 0.11 ms, $n = 11$ cells) when compared to controls (all $P > 0.05$, Fig. 2b).

Next, inhibitory glycinergic synaptic transmission was analysed by monitoring glycinergic (glyc-) mPSCs, recorded in the presence of picrotoxin (50 μM) to block GABAergic currents and kynurenic acid (2.5 mM) to block glutamatergic currents (Fig. 2c). We observed no changes in the frequency of glyc-mPSC in either s-GO (3.9 ± 0.5 Hz, $n = 15$ cells) or dfG injected fish (3.2 ± 0.5 Hz, $n = 11$ cells) when compared to controls (3.5 ± 0.5 Hz, $n = 14$ cells; $P > 0.05$; Fig. 2d). In addition, glyc-mPSC amplitudes (control: 33 ± 4 pA, dfG-injected: 34 ± 6 pA and s-GO-injected: 31 ± 4 pA), rise times (control: 0.43 ± 0.02 ms, dfG-injected: 0.4 ± 0.01 ms and s-GO-injected: 0.47 ± 0.03 ms) and
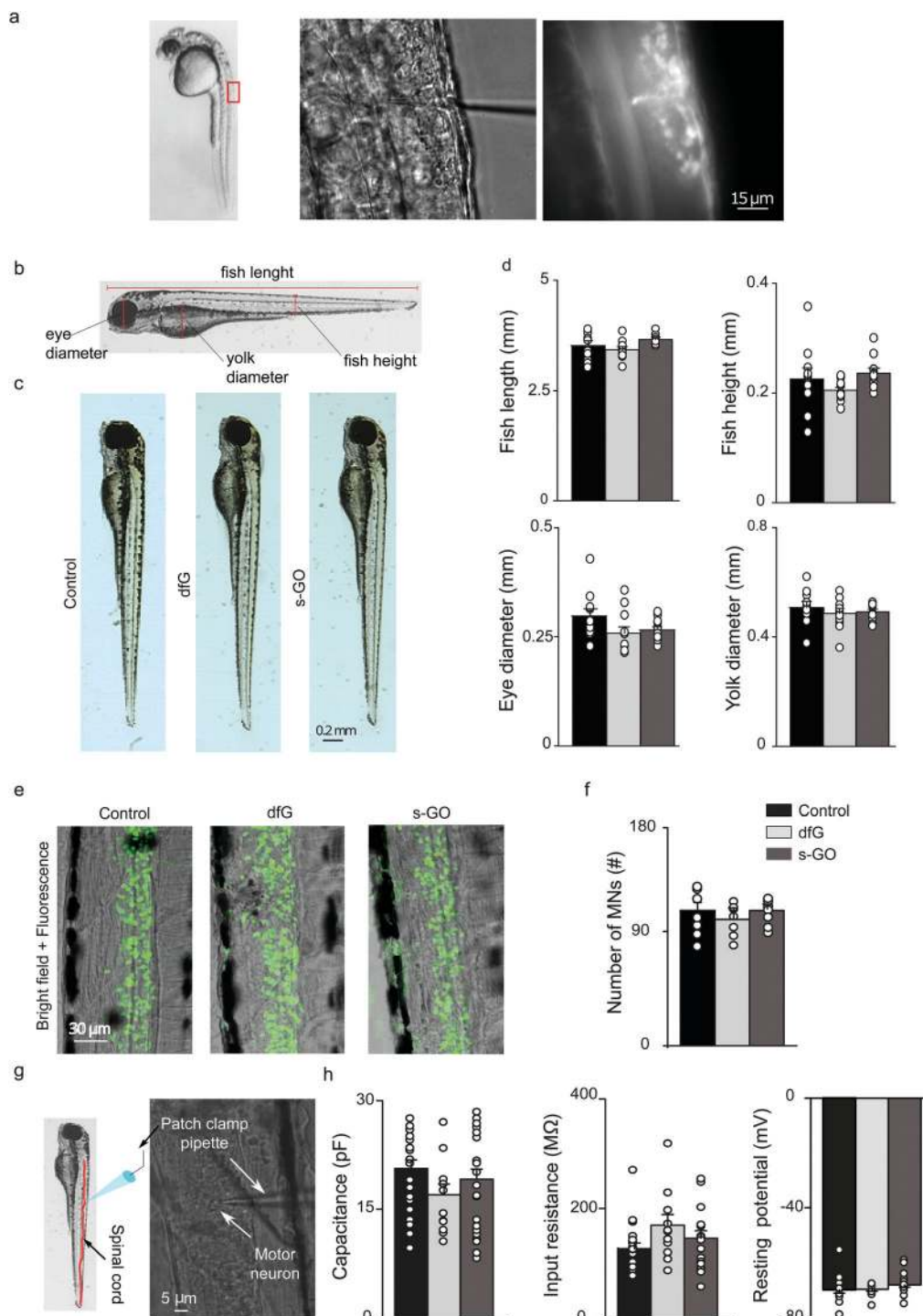
Fig. 1 Intra-spinal delivery of s-GO and dfG does not alter zebrafish development, neuronal survival or the electrophysiological basic properties of motor neurons. (a) Experimental setting for injections of nanomaterials in the spinal cord of 2 dpf zebrafish. Left: Lateral view of a 2 dpf zebrafish larva; the rectangle indicates the region of the body targeted by injection. Middle: Bright field image at higher magnification of the dorsal part of fish where solutions are delivered through a tiny glass pipette. Right: Fluorescence field of the previous image, showing that the injected solutions, added with a fluorescent dye, are delivered precisely in the spinal cord. (b) Schematic representation of the anatomical traits measured in zebrafish to analyse their development. (c) Bright field images of control, dfG-injected and s-GO-injected fish two days after injection. (d) Plots reporting the values of fish length and height, eye and yolk diameters. (e) Confocal images (Z-stack reconstructions) of the spinal cord of control, dfG-injected and s-GO-injected fish. Green signal is GFP expressed in motor neurons. (f) Plots reporting the number of motor neurons in the two segments of spinal cord around the site of injection. (g) Experimental setting for *in vivo* patch clamp recordings from motor neurons in zebrafish spinal cord: on the left a schematic representation of the patch clamp pipette inserted in the spinal cord (in red) of a larva, on the right bright field image of spinal neurons during recordings. A patch clamp pipette targeting the cell body of a motor neuron is visible. (h) Plots reporting the capacitance, the input resistance and the resting membrane potential of primary motor neurons. Dots superimposed to bars correspond to single fish or single neuron values.
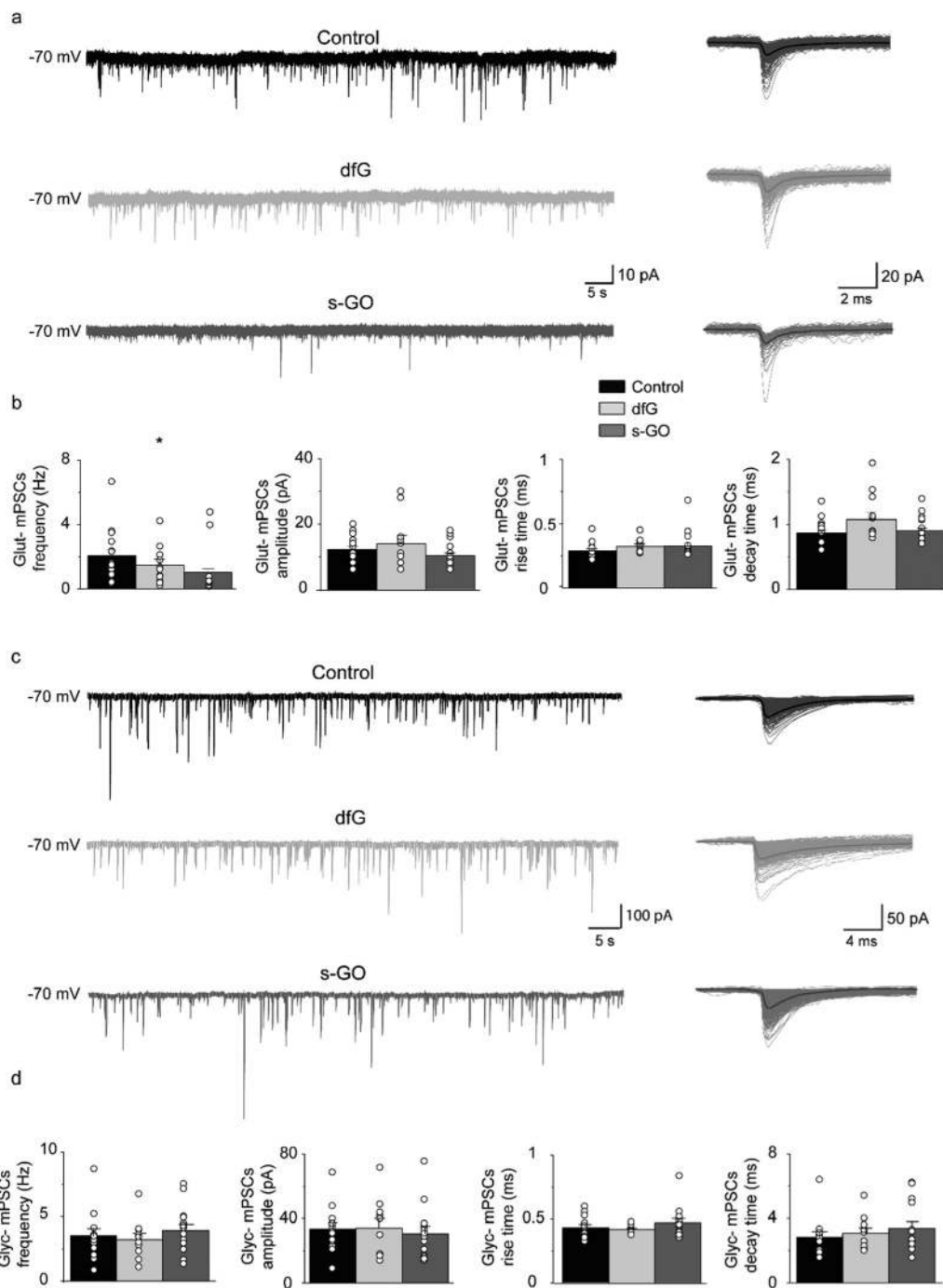
Fig. 2 Intra-spinal delivery of s-GO selectively impairs excitatory synapses. (a) Left panel: Sample tracings of glut-mPSCs recorded in control, dfG-treated and s-GO-treated fish. Right panel: glut-mPSCs collected from each corresponding trace and superimposed. Bold trace is the resulting electronic average. (b) Plots reporting the values of glut-mPSC frequency, amplitude, rise and decay time. (c) Left panel: Sample tracings of glyc-mPSCs recorded in control, dfG-treated and s-GO-treated fish. Right panel: glyc-mPSCs collected from each corresponding trace and superimposed. Bold trace is the resulting electronic average. (d) Plots reporting the values of glyc-mPSC frequency, amplitude, rise and decay time. Dots superimposed to bars correspond to single experiment values. s-GO treatment significantly decreased the frequency of glut-mPSCs (*$P < 0.05$).

decay times (control: 2.8 ± 0.3 ms, dfG-injected: 3.1 ± 0.3 ms and s-GO-injected: 3.4 ± 0.4 ms) did not significantly differ between treatment groups ($P > 0.05$, Fig. 2c and d). In sum, these findings suggest that s-GO, but not dfG, selectively depresses glutamatergic signalling in the zebrafish spinal cord.

2.4. s-GO impair glutamatergic drive to motor neurons during fictive swimming

To determine if s-GO also impaired glutamatergic signalling during locomotor-related network activity, synaptic input to motor neurons during fictive locomotion (that is, electrical

activity that correlates with bouts of locomotor behaviour in paralysed fish) was recorded (as shown in Fig. 1g).

During fictive swimming, motor neurons receive synaptic drive from glutamatergic and glycinergic neurons, which generates volleys of combined excitatory and inhibitory currents[42,43] (Fig. 3a). To study these current components, we voltage clamped primary motor neurons at the chloride and cationic reversal potentials to isolate glutamatergic and glycinergic currents respectively.[43,44]

During bouts of fictive swimming recorded from s-GO injected fish (Fig. 3b), we observed a reduction in the total area of the excitatory glutamatergic drive (control: $22\,722 \pm 5434$ pA

ms, $n = 19$ cells; s-GO-injected: 9037 ± 1360 pA ms, $n = 18$ cells; $P = 0.031$, Fig. 3d) that was coupled with a decrease in the frequency (control: 24.0 ± 6 Hz; s-GO-injected: 7 ± 1.5 Hz; $P = 0.013$) and amplitude (control: 16 ± 2 pA; s-GO-injected: 10 ± 1 pA; $P = 0.04$) of glutamatergic currents during bouts of locomotor drive. These modifications were specifically induced by s-GO, as animals injected with dfG showed no statistically significant difference in these parameters with respect to controls (area: $10\,071 \pm 1448$ pA ms; glutamatergic PSC frequency: 23 ± 8 Hz; tonic current amplitude: 15 ± 2 pA; $n = 9$ cells, P values > 0.05). By contrast, the duration of bouts of excitatory drive (control: 1.25 ± 0.21 s; dfG-injected: 0.75 ± 0.12 s;
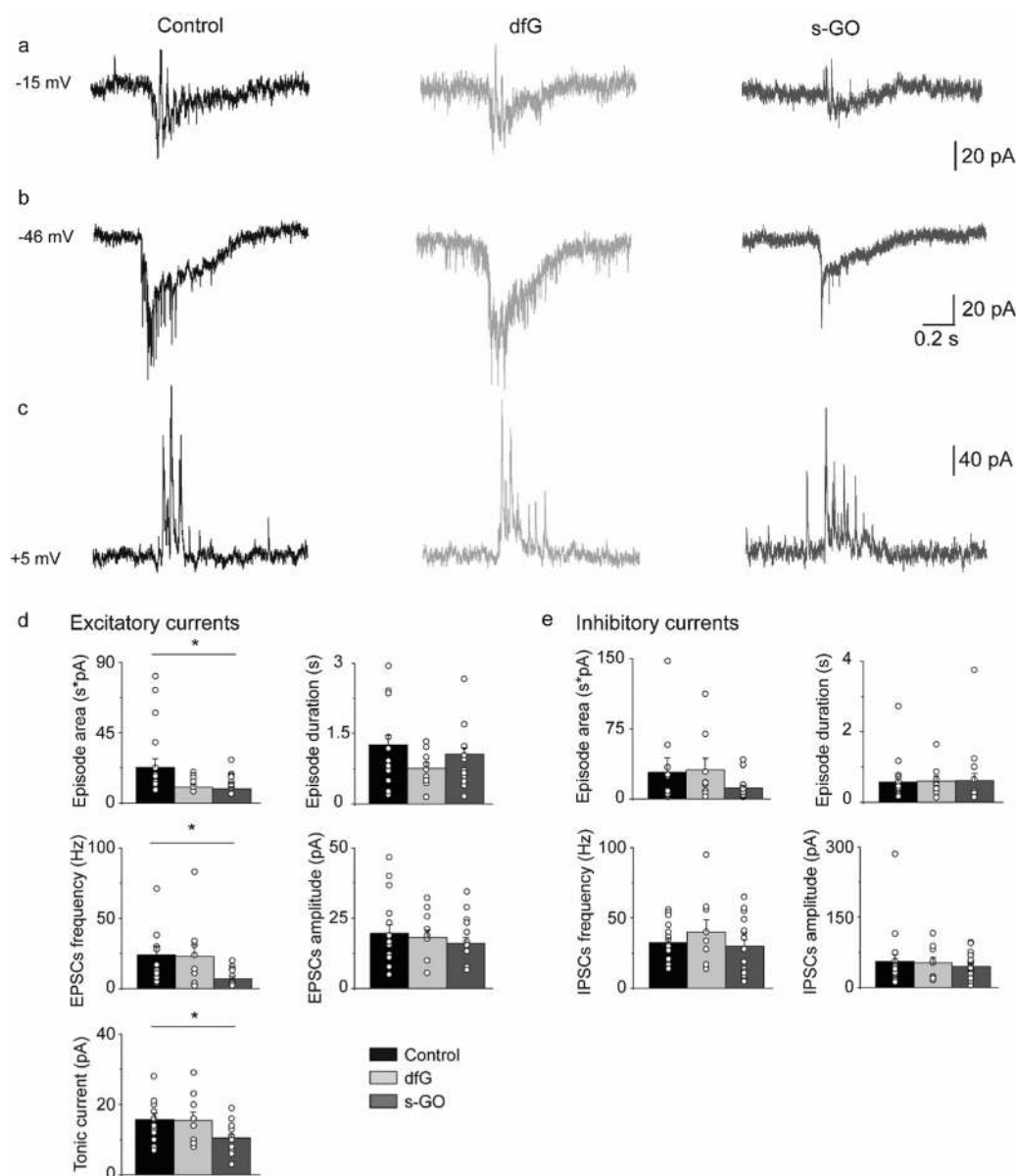
Fig. 3 Intra-spinal delivery of s-GO decreases the excitatory drive to motor neurons during fictive swimming. Examples of traces recorded at −15 mV (a), −46 mV (b) and +5 mV (c) for control (left), dfG-injected (middle) and s-GO-injected (right) fish. (d) Plots reporting the values of episode area and duration, EPSC frequency and amplitude, and tonic current amplitude for the excitatory drive. s-GO treatment significantly decreased the episode area, EPSC frequency and the tonic current (*P < 0.05). (e) Plots reporting the values of episode area and duration, IPSC frequency and amplitude, for the inhibitory drive. Dots superimposed to bars correspond to single experiments values.

s-GO-injected: 1.06 ± 0.14 s) and the amplitude of glutamatergic postsynaptic currents (control: 20 ± 3 pA, dfG-injected: 18 ± 3 pA; s-GO-injected: 16 ± 2 pA) were similar among the different groups ($P > 0.05$, Fig. 3d). These findings strongly suggest that s-GO, but not dfG, decrease the glutamatergic drive to motor neurons during fictive swimming.

The chloride-mediated glycinergic drive was also isolated by voltage clamping motor neurons at the reversal potential for cationic currents (Fig. 3c). In this case, no differences were detected in the area (control: 28 557 ± 15 391 pA ms, $n = 19$ cells; dfG-injected: 31 280 ± 12 067 pA ms, $n = 9$ cells; s-GO-injected: 11 727 ± 2621 pA ms, $n = 18$ cells; $P > 0.05$) or duration (control: 0.57 ± 0.13 s; dfG-injected: 0.59 ± 0.15 s; s-GO-injected: 0.61 ± 0.2 s) of the inhibitory bouts. Moreover, the amplitude (control: 56 ± 14 pA, dfG-injected: 53 ± 12 pA and s-GO-injected: 45 ± 6 pA) and the frequency (control: 33 ± 3 Hz, dfG-injected: 40 ± 9 Hz and s-GO-injected: 30 ± 5 Hz; P values > 0.5, Fig. 3e) of glycinergic PSCs during swim bouts were also not affected. Overall, these results point out that the glutamatergic, but not the glycinergic, locomotor drive to primary motor neurons is significantly reduced in zebrafish treated with s-GO.

2.5. s-GO injections in the spinal cord of the zebrafish impair locomotor performance

The analysis of synaptic drive to motor neurons during fictive swimming revealed that the excitatory inputs to motor neurons were depressed in s-GO injected fish. This suggested that intra-spinal delivery of this nanomaterial might also modify locomotor activity. This hypothesis was tested in two sets of behavioural experiments in which spontaneous and stimulus-evoked locomotor responses were analysed two days after treatment.

During spontaneous swimming tests (Fig. 4a), fish treated with s-GO exhibited a marked reduction in the total distance swum (110 ± 12 mm, $n = 16$ fish) in comparison to controls (378 ± 83 mm, $n = 11$ fish; $P = 0.0013$; Fig. 4a and b). This effect was mainly due to a statistically significant decrease in the length of the single bouts of swimming (control: 0.45 ± 0.04 s; s-GO-injected: 0.30 ± 0.03 s; $P = 0.022$), while the percentage of time spent active over the 5 min recording period was not changed between the different treatments (control: 20.6 ± 5.7%; s-GO-injected: 7.5 ± 1.6%; $P > 0.05$). Remarkably, dfG-treated larvae did not show any statistically significant difference in their locomotor activity with respect to controls (swim distance was 237 ± 65 mm, bout length was 0.35 ± 0.03 s and the percentage of motor activity was 15.7 ± 4.0%, $n = 13$ fish; P values > 0.5, Fig. 4a and b).

Startle-evoked locomotor responses were elicited by applying an acoustic stimulation to the recording chamber (Fig. 4c). In all the three conditions (control, dfG and s-GO treatments), fish showed a robust locomotor response immediately after the stimulus. However, locomotor duration (control: 9.98 ± 3.24 s, $n = 13$ fish; s-GO treated larvae: 1.45 ± 0.31 s, $n = 13$ fish; $P = 0.046$) and distance travelled (control: 44 ± 13 mm; s-GO-injected: 9 ± 2 mm; $P = 0.044$, Fig. 4c and d) were decreased in

fish injected with s-GO. By contrast, dfG injected fish did not exhibit statistically significant changes in these parameters (4.25 ± 1.47 s and 27 ± 7 mm, $n = 13$ fish; $P > 0.05$). The averaged velocity of swimming (calculated over the time of effective swimming) was comparable among the three groups (control: 5.6 ± 1.2 mm s^{-1}; dfG-injected: 8.1 ± 1.6 mm s^{-1} and s-GO-injected: 5.7 ± 1.3 mm s^{-1}; $P > 0.05$).

These findings indicate that swimming performance is markedly reduced in zebrafish treated with s-GO and, when considered in light of our electrophysiological results, are likely to arise from an impairment of the glutamatergic drive to motor neurons.

2.6. Graphene-based nanomaterials can be detected in the spinal cord after injection

We attempted to determine the presence of nanomaterials within the spinal cord of injected zebrafish. Both dfG and s-GO can be readily imaged when dispersed in saline solution using bright field light microscopy (Fig. 5a, left panels for each nanomaterial). However, due to the low intensity of contrast between the carbon backbone and the biological substrate, this technique is not informative to study nanomaterials in biological tissue. We therefore exploited the optical properties of both types of graphene-based materials to investigate their localization in zebrafish *in vivo*. dfG of larger size and thickness were visualized by reflected light imaging acquisition mode,[11] while s-GO were previously intracellularly tracked, utilizing their intrinsic fluorescent properties by confocal fluorescence microscopy.[45] The right panels of Fig. 5a show for each material how it appears when visualized in saline solution using these different imaging techniques.

Two days after the intra-spinal direct microinjection, zebrafish treated with dfG were scanned *in vivo*, both in fluorescence and reflective modes. Using reflection microscopy approaches, dfG were observed in the spine at around the site of delivery, indicating that at least the larger dfG flakes and their aggregates were still *in locus* two days after the post-injection (Fig. 5b). Zebrafish treated with s-GO were imaged using standard confocal microscopy. However, using this approach, we were unable to detect s-GO in the spinal cord 2 days after injection (Fig. 5c). Nonetheless, 1 day after the treatment the presence of the s-GO nanosheets was observed at the site of injection within the spinal cord (Fig. 5d).

3. Discussion

We report here the ability of s-GO nanosheets to modulate zebrafish spinal glutamatergic synapses and correlated locomotor behaviour *in vivo*. Remarkably, the effect was specific for this type of graphene-based material, since dfG with similar lateral dimensions did not induce any statistically significant modification in the electrical activity of spinal synapses, as well as in the behaviour of injected larvae with respect to controls. Our findings point towards a specific downregulation of synaptic signalling at glutamatergic synapses targeting motor neurons, as demonstrated by the decrease in excitatory
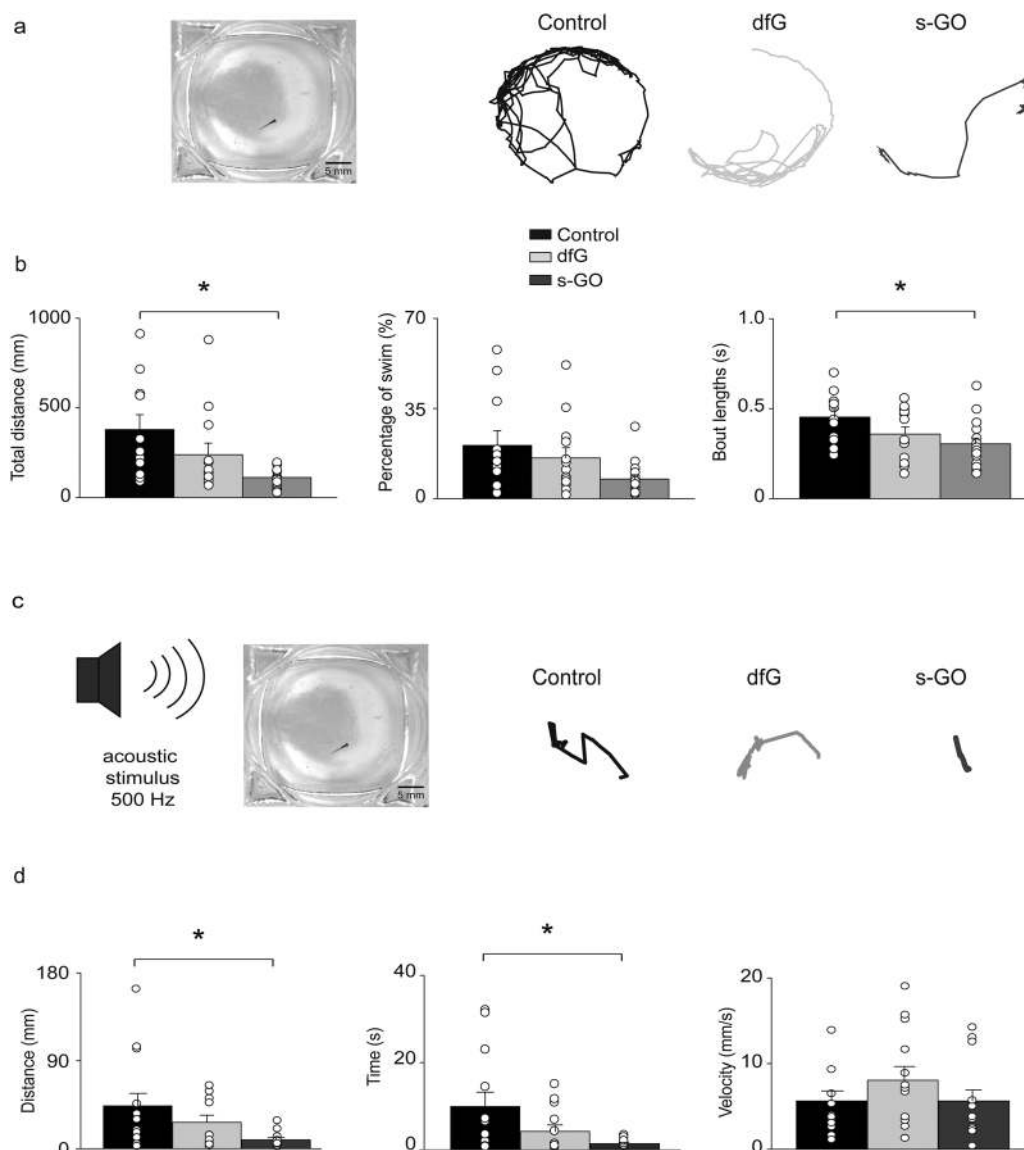
Fig. 4   Effects of intra-spinal delivery of s-GO on zebrafish behaviour. (a) Left: Bright field image of recording chamber for free swimming test. Right: Swimming trajectories of 4 dpf control, dfG-injected and s-GO-injected zebrafish recorded over a 5 min period. (b) Plots reporting the values of the total distance swum, percentage of time spent swimming and swimming bout length. Dots superimposed to bars correspond to single experiments values. s-GO treatment significantly decreased the total distance swum and the length of swimming bouts (*$P < 0.05$). (c) Left, sketch of the experimental setting in startle response experiments. Right, swimming trajectories of 4 dpf control, dfG injected and s-GO-injected zebrafish swum after the application of an acoustic stimulus. (d) Plots reporting the values of the distance swum, the time spent swimming and the swimming velocity. s-GO treatment significantly decreased the distance swum and the time spent swimming (*$P < 0.05$).

mPSCs frequency. This effect was also manifested as a reduction in the glutamatergic drive for locomotion during *in vivo* bouts of fictive locomotion. Such phenomenon did not appear to stem from a general perturbation of neuronal membrane properties as basic electrophysiological parameters of the neurons were not changed, reflecting neuronal health and membrane integrity.[39–41] In addition, the density of motor neurons, excitatory and inhibitory interneurons monitored by analysing the number of GFP positive cells in the site of the injection in different types of transgenic fish (Tg(hb9:GFP), Tg(GlyT2:GFP) and Tg(VGlut2A:GFP)) was not altered, demonstrating that s-GO do not affect neuronal survival.

The decrease in the frequency, but not in the amplitude, of glut-mPSCs observed in s-GO treatment is commonly associated with changes at the pre-synaptic loci.[46] These observations stand in broad agreement with previous studies carried on *in vitro*[10,11] and on brain explants obtained from animals injected with s-GO,[12] demonstrating a depression in glutamate vesicular release following s-GO exposure. One possible explanation for this effect is that nanomaterials in the synaptic cleft might trap glutamate releasing vesicles in an open state, preventing the re-cycling of synaptic vesicles.[10,12] If such hypothesis was confirmed, synaptic release over time would be expected to result in depletion of vesicles from the presynaptic
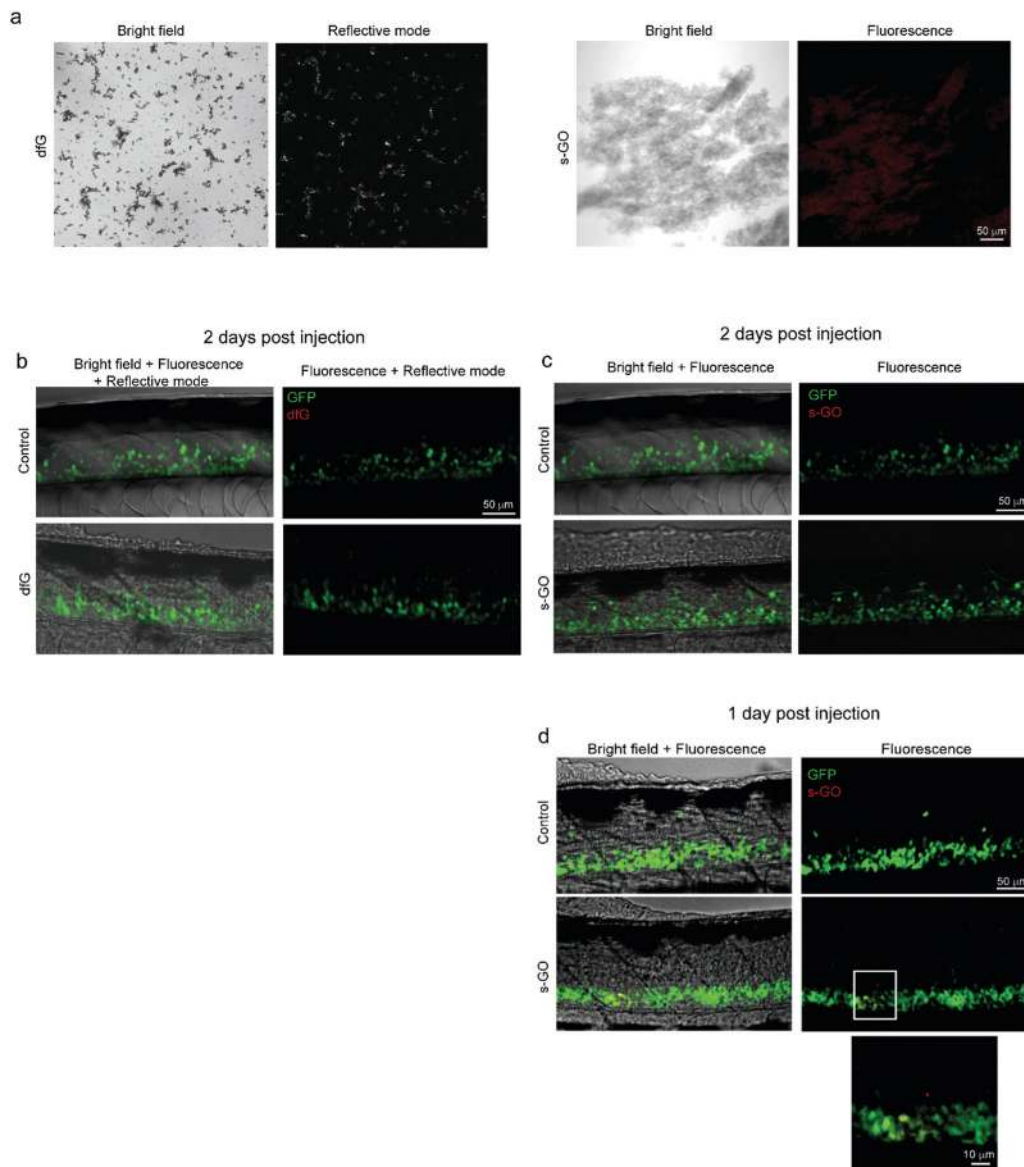
Fig. 5 Confocal microscopy of dfG and s-GO injected in the spinal cord of zebrafish. (a) Images of dfG and s-GO dispersed in saline solution. Left panels for each material are bright field images, while right panels are images in reflective mode for dfG and in fluorescence for s-GO. (b) Z-stack reconstructions of the spinal cord of control and dfG-injected fish, 2 days after treatment. Images, acquired in fluorescence and reflective modes sequentially, show the localization of dfG (red) in the spinal cord, which is identifiable thanks to the presence of GFP positive motor neurons (green). (c and d) Z-stack reconstructions of the spinal cord of control and s-GO-injected fish, 2 days (c) and 1 day (d) after treatment. Images, acquired in fluorescence mode sequentially for the red and green channels, show the localization of s-GO (red) in the spinal cord, which is identifiable thanks to the presence of GFP positive motor neurons (green), only 1 day after the injection (d), but not later (c). In (d), below, magnification of the area in the square for s-GO injected fish.

terminal. This would account for the reduction in excitatory synaptic drive during recordings of fictive locomotor activity.[47]

In contrast to our findings with s-GO, we observed no change in mPSC properties or locomotor-related synaptic signalling following dfG spinal cord injection. Although investigation of the mechanisms underlying the interaction between s-GO and synaptic vesicles is beyond the scope of this study, we can speculate that the differential effects between these nanomaterials might arise from slight differences in shape and thickness which in turn would affect nanoparticle–membrane interactions.[48] In addition, the thinner, more hydrophilic character of s-GO, presenting many more oxygen-rich surface functionalities, not only favours the dispersibility of the nanosheets in saline solution,[49] but also allows for more complex interactions with neuronal components (ion channels, clefts), and in particular those at the plasma membrane.

Our behavioural studies detected a diminished locomotor performance in zebrafish treated with s-GO, both in free and evoked swimming tests. It is unlikely that this effect arises from a developmental delay as the quantitative analysis of

anatomical features commonly used as indicators of zebrafish development,[34] suggested that s-GO injection did not perturb development. Alterations in neuronal growth are also unlikely as electrophysiological passive properties of neurons were not affected by s-GO injection.[39–41]

Therefore, the observed reduction in locomotor activity of s-GO-injected larvae stems from a decreased excitatory drive to motor neurons in the spinal network. Assuming that integrative properties of motor neurons are not modified, the s-GO induced reduction of excitatory drive, in the presence of no changes in the inhibitory inputs, is expected to lead to decrease in motor neuron drive, which in turn will decrease activation of muscle fibers. This is compatible with the reduction in the locomotor performance observed in our behavioural studies. Remarkably, the analysis of free swimming activity has revealed a reduction in the length of single swimming bouts and, as a consequence, in the distance swum by larvae injected with s-GO nanosheets. Similarly, stimulus-evoked startle responses appeared shorter in duration and distance covered in animals treated with s-GO. We speculate that such behaviour might correlate with a reduced availability of glutamate in the pre-synaptic terminal.

Our results might appear in contrast with recent works reporting developmental neurotoxic effects of graphene oxide in zebrafish larvae and embryos.[50–52] However, differences in the characteristics of the used nanomaterial (e.g. the lateral size), in its preparation method or in the modality of zebrafish exposure might be responsible for such diverse outcome. A detailed physico-chemical characterization of nanomaterials, as the one we reported here, is fundamental for understanding the biological effect of specific types of nanostructured materials.[53]

In relation to a previous report where the impairment of rat excitatory synapses due to in vivo s-GO exposure was shown,[12] our findings offer new knowledge on how s-GO interference with glutamatergic synapses in a specific brain region can result in modulation of animal behaviour that relies on the activity of that neuronal network. In our model neuronal activity from an intact spinal network connected with other regions of the nervous system (e.g. sensory system) was recorded in an in vivo setting. This allowed a more comprehensive understanding of the effect of nanomaterials on neuronal network signals ongoing in vivo (fictive swimming) and driving locomotor behaviour.

Fluorescence and light-reflective microscopy is a reliable qualitative technique to image graphene-based nanomaterials in biological tissue[11,45,54] and through these approaches we attempted to detect the presence of dfG and s-GO sheets in zebrafish in vivo post-injection. At two days post-injection, when s-GO mediated electrophysiological and behavioural effects were observed, we could image dfG, but not s-GO locally. Nevertheless, we were able to detect the presence of s-GO in the spinal cord 24 hours after the injection. This finding confirms that s-GO were effectively delivered to the spinal cord and localized within the nervous system for at least 24 hours. It remains to be determined why s-GO sheets were no longer

observed at later stages. This could be because s-GO diffused, or were actively cleared, from the site of injection, resulting in levels of concentration or focal aggregation that fell beyond the limits of detection for the microscopic technique used (spatial resolution in the range of 1–2 μm for intact zebrafish[55,56]). Our electrophysiological experiments were not able to dissect if the observed reduction in excitatory signalling resulted from the direct presence of s-GO in the spinal cord, (but at low, undetectable, concentration), or if two days after injections the nanomaterial was completely cleared. In this last hypothesis, the decrease in excitatory transmission could arise from the effect of s-GO during the maturation of synaptic circuitry, resulting in the consolidation of glutamatergic synapses with a reduced release of neurotransmitter from presynaptic terminals. Future investigations will be required to validate this possibility.

4. Conclusion

We have shown here that intra-spinally injected s-GO in zebrafish depress glutamatergic transmission in vivo and result in modifications of animal behaviours which are associated with neuronal network activity of the spinal cord. These findings, considered in conjunction with previous reports of the s-GO effect observed in rat hippocampal and cortical preparations[10–12] suggest that these thin nanosheets can induce inhibition of glutamatergic signalling ubiquitously across brain circuits and animal species. Such findings may pave the way towards the translation of s-GO in therapy for the treatment of human nervous system diseases in which excitatory transmission is pathologically increased.

5. Experimental

5.1. Preparation and physicochemical characterization of s-GO and dfG

Previously established protocols were used to produce s-GO[10,29–31] and dfG.[32,33] A detailed description of these and the physicochemical characterization of the two nanomaterials are reported in ESI.†

5.2. Intra-spinal delivery of nanomaterials

Zebrafish (D. rerio) were maintained and treated at the University of Leicester (UK) in accordance with the local, national (Animals Act 1986, Scientific Procedures) and E.U. guidelines for animal welfare. The work was approved by the university Animal Welfare and Ethical Review Body and by the Genetic Modification Committee. Zebrafish larvae aged 2 dpf were anesthetised with 0.02% MS222 (Sigma) and embedded 2% agarose. Fine glass pipettes (diameter < 1 μm) were filled with control or nanomaterial containing solution which was then inserted into the 7th–8th segments of the spinal cord using a 10× objective of an upright microscope equipped with epifluorescence system (Nikon, Eclipse FN1). Approximately 0.5 nl, corresponding to ~0.5 μg of nanomaterial containing

solution was ejected from the pipette using a pressurized air microinjector (Picosprizter III, 12 ms duration, 10 PSI). Three solutions were used for injections: (1) control standard saline solution (Evan's solution, whose composition is described below), (2) dfG containing solution (dissolved in saline solution at a concentration of 0.9 mg ml^{-1}) and (3) s-GO containing solution (dissolved in saline solution at a concentration of 0.9 mg ml^{-1}). A fluorescent dye (Alexa Fluor 488) was included in the injection solution to facilitate visualisation of the site of injection and the effective delivery of the solution.

After injections, larvae were carefully removed from agar with fine forceps, immersed in Evan's solution and allowed to recover in standard conditions (at 28.5 °C on a 14 : 10 hour light : dark cycle) until reaching the age of 4 dpf.

5.3. Morphological analysis of larvae

For morphological analysis, 4 dpf larvae were anesthetised with 0.02% of MS222 and fixed with PFA 4% (Sigma) for 90 min a room temperature. Fixed animals were put on a plastic dish in PBS and imaged with a microscope (Nikon 8M7800) interfaced to camera (Moticam 1000) and an acquisition software (Image Plus 2.0). The following anatomical traits were measured to evaluate the developmental stage: larvae length was the distance from the snout to the caudal peduncle. Larvae height was the distance from ventral to dorsal, defined ventrally by the confluence of the anterior margin of the anal fin, the posterior of the peritoneal cavity and the ventral margin of the myotomes. Eye diameter was the distance at the longest axis of the eye. Yolk diameter was the distance at the shorter axis of the yolk.[34]

5.4. Confocal microscopy

To quantify neuron numbers transgenic zebrafish expressing GFP selectively in motor neurons, excitatory and inhibitory interneurons were used (Tg(hb9:GFP), Tg(glyT2:GFP) and Tg(VGLUT2A:GFP)).[35,36] Larvae at 4 dpf were fixed in PFA, rinsed in PBS and cleared in glycerol prior to mounting on microscopy slides.

The spinal cord was imaged at a magnification of 40× on an Olympus FV1000 confocal laser scanning microscope using Fluoview FV1000 capture software and serial confocal planes were acquired every 0.5 μm across the spine of the fish. For imaging of GFP expression in neurons, an excitation wavelength of 488 nm and filters for an emission wavelength of 495–530 nm were used. Reconstructions of the images were performed offline using the image-processing package Fiji. The number of GFP positive motor neurons was counted from z-stack images using the Cell counter plugin for Fiji. For imaging of nanomaterials injected in the spinal cord, larvae were anesthetised with 0.02% of MS222, embedded in agar 2% and mounted on microscopy slides. Excitation/emission wavelengths for GFP was as reported above. Excitation wavelength for s-GO was 594 nm, while emission wavelength was 620–700 nm. The acquisition was performed in a sequential mode for the two channels. dfG were visualised by using the reflection mode property during the confocal acquisition. The same acquisition setting was used for nanomaterials injected fish and controls, to avoid artefactual signals.

5.5. Electrophysiology

Whole cell voltage clamp recordings were conducted in 4 dpf zebrafish larvae *in vivo* as previously described.[42] After being anesthetized and paralyzed in Evans physiological saline (134 NaCl, 2.9 KCl, 2.1 CaCl$_2$, 1.2 MgCl$_2$, 10 mM glucose and 10 HEPES, pH 7.8) containing 0.02% tricaine (MS-222), larvae were pinned on their side to the surface of a Sylgard-coated plastic Petri dish by pressing short pieces of fine tungsten wire through the notochord. To expose the spinal cord, the skin between the two pins was removed using suction through a patch pipette with the tip diameter of ~50 μm. Suction was used initially to remove the skin from the muscle underneath while the pipette was moved caudally over the trunk. Through a similar procedure, muscles were removed as well, making the spinal cord accessible for a length of 2–3 somites. At this point, fish were perfused with Evans physiological saline containing the neuromuscular blocker D-tubocurarine (10 μM). All electrophysiological recordings were performed at room temperature. A cell body in the spinal cord was approached while a small amount of positive pressure in the patch pipette was applied, in order to break the dura overlying the spinal cord, leaving the naked cell body of neuron exposed to the pipette.

Patch clamp recordings were performed from primary motor neurons of Tg(hb9:GFP) zebrafish larvae, which were identified by means of their GFP expression and their stereotyped cell-body positions and size.[37]

Patch electrodes, pulled from borosilicate glass capillaries (Harvard Apparatus, UK), with a resistance of 7–10 MΩ were used for electrophysiology recording. For most experiments, these were filled with intracellular solution containing (in mM) K gluconate 126, KCl 16, MgCl$_2$ 2, HEPES 10, EGTA 10 and Na$_2$ATP 4 (pH 7.3). However, for recordings of glyc-mPSCs, a high chloride electrode solution was used that contained (in mM) CsCl 135, HEPES 10, EGTA 10, Na$_2$ATP 2, MgCl2 2 (pH 7.3). Sulforhodamine B (0.1%) was routinely added to the patch pipette solution to visualise neuronal morphology using fluorescence optics of the patch clamp microscope (Nikon FN-1). This permitted to confirm cell phenotype on the base of characteristic peripheral branching patterns.[38] For all recordings, a patch-clamp amplifier (Multiclamp 700B, Axon Instruments, Sunnyvale, CA, USA) connected to an analog to digital converter (Digidata 1440A, Axon Instruments, Sunnyvale, CA, USA) was used to acquire electrophysiology data which were stored on a PC running pClamp 10, Axon Instruments, Sunnyvale, CA, USA. Raw signals were acquired at 10 kHz and filtered offline at 2 kHz. Liquid junction potential was of ~13 mV (calculated with the Clampex software; Molecular Devices, Sunnyvale, CA, USA) and membrane potentials were corrected for it.

Immediately after getting the whole cell configuration, resting membrane potentials were recorded in current clamp mode setting the holding current at zero ($I = 0$).

All the other measurements were carried out in voltage clamp mode. Glut-mPSCs and gly-mPSCs were recorded from

a holding potential of -70 mV in the presence of TTX (1 μM, to block sodium currents and propagated action potentials), picrotoxin (50 μM, to abolish $GABA_A$ receptor mediated currents), and either strychnine (1 μM, to block glycinergic currents) or kynurenic acid (2.5 mM, to block glutamatergic currents).

To isolate excitatory inputs to primary motor neurons during fictive swimming, cells were clamped at the reversal potential of chloride (-46 mV), while to record inhibitory input, the holding potential was set at the reversal potential for cationic currents ($\sim +5$ mV).

The stability of the patch was checked by repetitively monitoring the input and series resistance during the experiments. Cells exhibiting 15% changes were excluded from the analysis. The series resistance was < 20 MΩ and it was not compensated.

5.6. Electrophysiological data analysis

Input resistance and cells capacitance were measured online with the membrane test feature of the pClamp software.

For analysis of glut- and gly-mPSC, template matching functions[10–12] were used to isolate populations of events. The frequency of mPSCs was calculated as the number of events in a 300 second period. For each recording, mPSCs were averaged, then the rise time (defined as the time taken by the current to go from the 10% to the 90% of the peak value), the decay time (corresponding to the time required by the current to decline from the 90% to 10% of the peak value) and amplitude of mPSCs were examined in the resulting trace. The data obtained from different cells were averaged across each experimental condition. The decay phase of miniature PSCs was calculated from averaged traces by fitting it with a mono-exponential function.

For the analysis of fictive swimming, the duration, the area and the amplitude of tonic current in episodes of excitatory and inhibitory drive were measured manually with cursors. Glutamatergic and glycinergic post synaptic currents (PSCs) during the episodes were detected using the template function of Clampfit and their frequency and amplitude were measured. For each cell, at least six bouts of excitation and six bouts of inhibition were considered.

5.7. Drug treatment

Drugs were applied to the bath *via* a gravity-fed perfusion system. Drugs used were: strychnine and picrotoxin, purchased from Sigma-Aldrich (UK), kynurenic acid and TTX from Hello-Bio (UK). Stock solutions were made in distilled water or in DMSO and then aliquoted and frozen at $-20\ ^\circ$C.

5.8. Behavioural experiments

For free swimming experiments, individual 4 dpf larvae were transferred to a recording chamber that contained an overhead camera and an infrared light source for illumination. Fish were allowed to acclimatize for 10 minutes before behaviour was recorded for a period of 5 minutes.

To measure the startle response, after 5 minutes of acclimatization, escape swimming was elicited by applying an acoustic stimulation to the recording chamber. The acoustic stimulation was a computer generated sudden loud noise (1 tone at 500 Hz, lasting 1 second), played through a commercial loudspeaker, which was physically connected to the recording chamber. The sound intensity in proximity of the recording chamber was measured with a noise detector and was ~ 70 dB.

Digital video (avi format) recordings were acquired at 15 frames per second using Flycap2 software (Point Grey). Files were then processed in VirtualDub and converted to the micro fly movie format (ufmf) using any2ufmf (http://ctrax.source forge.net/any2ufmf.html) for subsequent analysis in California Institute of Technology Fly Tracker (Ctrax, v 0.2.16). The position and orientation of individual fish was quantified in a semi-automated manner by Ctrax. Errors in tracking were subsequently corrected using FixErrors in MatLab environment. The velocity of swimming and distance swum were extracted with this analysis.

In addition, the number and the duration of beat/glide episodes during free swimming were measured by means of The Janelia Automatic Animal Behavior Annotator (JAABA; http://jaaba.sourceforge.net/).

5.9. Statistics

The results are presented as the mean $\pm$ SE; n is the number of neurons for patch clamp experiments and of fish for anatomical and behavior studies. Statistical analysis was performed by using the software Prism GraphPad 8. Data were first tested for normality by using Shapiro–Wilk test. For parametric data, the statistically significant difference among the three groups was assessed through one-way ANOVA, using Tukey's test for *post hoc* analysis. Not parametric data were analyzed with Kruskal–Wallis test and *post hoc* analysis was done with Dunn' multiple comparison test. Reported P values are those calculated in the *post hoc* analysis. $P < 0.05$ was considered statistically significant.

Conflicts of interest

There are no conflicts of interest to declare.

Acknowledgements

References

1 K. S. Novoselov, V. I. Fal'ko, L. Colombo, P. R. Gellert, M. G. Schwab and K. Kim, *Nature*, 2012, **490**, 192.

2 H. Y. Mao, S. Laurent, W. Chen, O. Akhavan, M. Imani, A. A. Ashkarran and M. Mahmoudi, *Chem. Rev.*, 2013, **113**, 5.

3 K. Kostarelos and K. S. Novoselov, *Nat. Nanotechnol.*, 2014, **9**, 10.

4 K. S. Novoselov, A. K. Geim, S. V. Morozov, D. Jiang, Y. Zhang, S. V. Dubonos, I. V. Grigorieva and A. A. Firsov, *Science*, 2004, **306**, 5696.

5 K. S. Novoselov, D. Jiang, F. Schedin, T. J. Booth, V. V. Khotkevich, S. V. Morozov and A. K. Geim, *Proc. Natl. Acad. Sci. U. S. A.*, 2005, **102**, 30.

6 A. K. Geim, *Science*, 2009, **324**, 5934.

7 K. Kostarelos and K. S. Novoselov, *Science*, 2014, **344**, 6181.

8 D. Bitounis, H. Ali-Boucetta, B. H. Hong, D. H. Min and K. Kostarelos, *Adv. Mater.*, 2013, **25**, 16.

9 D. Kuzum, H. Takano, E. Shim, J. C. Reed, H. Juul, A. G. Richardson, J. de Vries, H. Bink, M. A. Dichter, T. H. Lucas, D. A. Coulter, E. Cubukcu and B. Litt, *Nat. Commun.*, 2014, **5**, 5259.

10 R. Rauti, N. Lozano, V. León, D. Scaini, M. Musto, I. Rago, F. P. Ulloa Severino, A. Fabbro, L. Casalis, E. Vázquez, K. Kostarelos, M. Prato and L. Ballerini, *ACS Nano*, 2016, **10**, 4.

11 M. Bramini, S. Sacchetti, A. Armirotti, A. Rocchi, E. Vázquez, V. León Castellanos, T. Bandiera, F. Cesca and F. Benfenati, *ACS Nano*, 2016, **10**, 7.

12 R. Rauti, M. Medelin, L. Newman, S. Vranic, G. Reina, A. Bianco, M. Prato, K. Kostarelos and L. Ballerini, *Nano Lett.*, 2019, **19**, 5.

13 Y. Zhou and N. C. Danbolt, *J. Neural Transm.*, 2014, **121**, 8.

14 J. Lewerenz and P. Maher, *Front. Neurosci.*, 2015, **16**, 9.

15 X. Dong, Y. Wang and Z. Quin, *Acta Pharmacol. Sin.*, 2009, **30**, 379.

16 B. M. Cortese and K. L. Phan, *CNS Spectr.*, 2005, **10**, 10.

17 B. S. Meldrum, *Neurology*, 1994, **44**, 11.

18 G. Ambrosi, S. Cerri and F. Blandini, *J. Neural Transm.*, 2014, **121**, 8.

19 A. E. King, A. Woodhouse, M. T. Kirkcaldie and J. C. Vickers, *Exp. Neurol.*, 2016, **275**, 1.

20 J. P. Briggs, *Am. J. Physiol.: Regul., Integr. Comp. Physiol.*, 2002, **282**, 1.

21 R. W. Friedrich, G. A. Jacobson and P. Zhu, *Curr. Biol.*, 2010, **20**, 8.

22 K. E. Lewis and J. S. Eisen, *Prog. Neurobiol.*, 2003, **69**, 6.

23 P. Z. Myers, *J. Comp. Neurol.*, 1985, **236**, 4.

24 M. E. Hale, D. A. Ritter and J. R. Fetcho, *J. Comp. Neurol.*, 2001, **437**, 1.

25 S. Higashijima, G. Mandel and J. R. Fetcho, *J. Comp. Neurol.*, 2004, **480**, 1.

26 J. R. Fetcho, *J. Exp. Zool., Part B*, 2007, **308**, 550–562.

27 J. R. Fetcho, S. Higashijima and D. L. McLean, *Brain Res. Rev.*, 2008, **57**, 1.

28 R. W. Friedrich, G. A. Jacobson and P. Zhu, *Curr. Biol.*, 2010, **20**, 8.

29 D. A. Jasim, N. Lozano and K. Kostarelos, *2D Mater.*, 2016, **3**, 014006.

30 S. P. Mukherjee, N. Lozano, M. Kucki, A. E. Del Rio-Castillo, L. Newman, E. Vázquez, K. Kostarelos, P. Wick and B. Fadeel, *PLoS One*, 2016, **11**, e0166816.

31 Y. Hernandez, V. Nicolosi, M. Lotya, F. M. Blighe, Z. Sun, S. De, M. T. B. Holland, M. Byrne, Y. K. Gun'Ko, J. J. Boland, P. Niraj, G. Duesberg, S. Krishnamurthy, R. Goodhue, J. Hutchison, V. Scardaci, A. C. Ferrari and J. N. Coleman, *Nat. Nanotechnol.*, 2008, **3**, 9.

32 H. Yang, Y. Hernandez, A. Schlierf, A. Felten, A. Eckmann, S. Johal, P. Louette, J.-J. Pireaux, X. Feng, K. Mullen, V. Palermo and C. Casiraghi, *Carbon*, 2013, **53**, 03.

33 A. F. Rodrigues, L. Newman, N. Lozano, S. P. Mukherjee, B. Fadeel, C. Bussy and K. Kostarelos, *2D Mater.*, 2018, **5**, 035020.

34 D. M. Parichy, M. R. Elizondo, M. G. Mills, T. N. Gordon and R. E. Engeszer, *Dev. Dyn.*, 2009, **238**, 12.

35 T. Nakano, M. Windrem, V. Zappavigna and S. A. Goldman, *Dev. Biol.*, 2005, **283**, 2.

36 C. Satou, Y. Kimura, H. Hirata, M. L. Suster, K. Kawakami and S. Higashijima, *Development*, 2013, **140**, 18.

37 M. Westerfield, J. V. McMurray and J. S. Eisen, *J. Neurosci.*, 1986, **6**, 8.

38 R. L. Moreno and A. B. Ribera, *J. Neurophysiol.*, 2009, **102**(4), 2477.

39 J. S. Carp, *J. Neurophysiol.*, 1992, **68**, 1121–1132.

40 Y. Gao, L. Liu, Q. Li and Y. Wang, *Neurosci. Lett.*, 2015, **591**, 138–143.

41 U. Djuric, A. Y. Cheung, W. Zhang, R. S. Mok, W. Lai, A. Piekna, J. A. Hendry, P. J. Ross, P. Pasceri, D. S. Kim, M. W. Salter and J. Ellis, *Neurobiol. Dis.*, 2015, **76**, 37–45.

42 P. Drapeau, D. W. Ali, R. R. Buss and L. Saint-Amant, *J. Neurosci. Methods*, 1999, **88**, 1.

43 R. R. Buss and P. Drapeau, *J. Neurophysiol.*, 2001, **86**, 1.

44 H. Tong and J. R. McDearmid, *Curr. Biol.*, 2012, **22**, 24.

45 S. Vranic, A. F. Rodrigues, M. Buggio, L. Newman, M. R. H. White, D. Spiller, C. Bussy and K. Kostarelos, *ACS Nano*, 2018, **12**, 2.

46 B. N. Queenan, K. J. Lee and D. T. Pak, *Neural Plast.*, 2012, **2012**, 718203.

47 E. D. Nelson, E. T. Kavalali and L. M. Monteggia, *J. Neurosci.*, 2008, **28**, 2.

48 J. Mao, R. Guo and L. T. Yan, *Biomaterials*, 2014, **35**, 23.

49 R. N. Jana and S. C. Chandra Ray, *Carbon nanomaterials for biological and medical applications*, Elsevier, Health Sciences Division, USA, 2017.

50 J. C. Soares, T. Pereira, K. M. Costa, T. Maraschin, N. R. Basso and M. R. Bogo, *Colloids Surf., B*, 2017, **157**, 335–346.

51 X. Yang, Q. Yang, G. Zheng, S. Han, F. Zhao, Q. Hu and Z. Fu, *Environ. Toxicol.*, 2019, **34**, 4.

52 C. Ren, X. Hu and Q. Zhou, *Adv. Sci.*, 2018, **5**, 1700595.

53 P. Wick, A. E. Louw-Gaume, M. Kucki, H. F. Krug, K. Kostarelos, B. Fadeel, K. A. Dawson, A. Salvati, E. Vázquez and L. Ballerini, *et al.*, *Angew. Chem., Int. Ed.*, 2014, **53**, 7714.

54 S. Bosi, R. Rauti, J. Laishram, A. Turco, D. Lonardoni, T. Nieus, M. Prato, D. Scaini and L. Ballerini, *Sci. Rep.*, 2015, **5**, 9562.

55 K. Stoletov, V. Montel, R. D. Lester, S. L. Gonias and R. Klemke, *Proc. Natl. Acad. Sci. U. S. A.*, 2007, **104**, 17406.

56 S. Karthik, T. Djukic, J. Kim, B. Zuber, A. Makanya, A. Odriozola, R. Hlushchuk, N. Filipovic, S. Won Jin and V. Djonov, *Sci. Rep.*, 2019, **9**, 4152.